Oxyhydride Nature of Rare-Earth-Based Photochromic Thin Films

Cornelius, Steffen; Colombi, Giorgio; Nafezarefi, Fahimeh; Schreuders, Herman; Heller, René; Munnik, Frans; Dam, Bernard

DOI
10.1021/acs.jpclett.9b00088

Publication date
2019

Document Version
Final published version

Published in
Journal of Physical Chemistry Letters

Citation (APA)
Cornelius, S., Colombi, G., Nafezarefi, F., Schreuders, H., Heller, R., Munnik, F., & Dam, B. (2019). Oxyhydride Nature of Rare-Earth-Based Photochromic Thin Films. *Journal of Physical Chemistry Letters*, *10*(6), 1342-1348. https://doi.org/10.1021/acs.jpclett.9b00088

THE JOURNAL OF PHYSICAL CHEMISTRY Letters

Letter

Cite This: J. Phys. Chem. Lett. 2019, 10, 1342−1348

pubs.acs.org/JPCL

Oxyhydride Nature of Rare-Earth-Based Photochromic Thin Films

Steffen Cornelius,*[,†] Giorgio Colombi,[†] Fahimeh Nafezarefi,[†] Herman Schreuders,[†] René Heller,[‡] Frans Munnik,[‡] and Bernard Dam[†]

[†]Materials for Energy Conversion and Storage, Department of Chemical Engineering, Delft University of Technology, Van der Maasweg 9, NL-2629HZ Delft, The Netherlands

[‡]Helmholtz-Zentrum Dresden-Rossendorf, Institute of Ion Beam Physics and Materials Research, Bautzner Landstrasse 400, D-01328 Dresden, Germany

Supporting Information

ABSTRACT: Thin films of rare-earth (RE)−oxygen−hydrogen compounds prepared by reactive magnetron sputtering show a unique color-neutral photochromic effect at ambient conditions. While their optical properties have been studied extensively, the understanding of the relationship between photochromism, chemical composition, and structure is limited. Here we establish a ternary RE−O−H composition-phase diagram based on chemical composition analysis by a combination of Rutherford backscattering and elastic recoil detection. The photochromic films are identified as oxyhydrides with a wide composition range described by the formula REO_xH_{3-2x} where $0.5 \leq x \leq 1.5$. We propose an anion-disordered structure model based on the face-centered cubic unit cell where the O^{2-} and H^- anions occupy tetrahedral and octahedral interstices. The optical band gap varies continuously with the anion ratio, demonstrating the potential of band gap tuning for reversible optical switching applications.

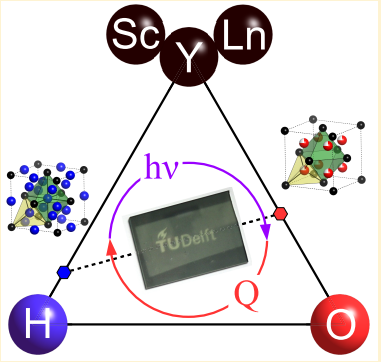

While the structure−property relationships of *single-anion* materials, such as metal oxides, are to a large extent determined by variations in the cation chemistry, *multianion* compounds offer another dimension of control of material properties. This is due to the wide range of different anion characteristics, including electronegativity, polarizability, and ionic radius.[1] Perhaps the least studied group of multianion compounds are oxyhydrides where both oxide (O^{2-}) and hydride (H^-) ions are present. Since the successful synthesis of the transition metal (TM) oxyhydride $LaSrCoO_3H_{0.7}$ by Hayward et al.,[2] this material class has been extended to TM = Sc, Ti, V, Cr, Mn, Co based on the perovskite and the layered Ruddlesden−Popper crystal structure types.[3] A recent report on hydride ion (H^-) conductivity in $La_{2-x-y}Sr_{x+y}Li_{1-x}HO_{3-y}$ makes oxyhydrides promising materials for energy storage and conversion applications.[4] Two synthesis routes for TM oxyhydrides have been established to date. Topochemical synthesis exploits the O^{2-}/H^- anion exchange between the parent oxide and a hydride (mostly CaH_2) at moderate temperatures of 300−600 °C.[3] Alternatively, some TM oxyhydrides have been prepared by high-pressure (few GPa) direct synthesis from parent oxide and hydride powder mixtures at 1000−1300 °C.[3] These methods have also been employed to synthesize powders of lanthanide (Ln) oxyhydrides LnOH with Ln = La,[5] Nd,[6] Sm,[7,8] Gd−Er[7−9], the second established class of oxyhydride materials. The stoichiometric LnOH are reported to crystallize either in the anion-disordered face-centered cubic (fcc) fluorite type structure ($Fm\bar{3}m$)[7−9] or in an anion-ordered superstructure with tetragonal ($P4/nmm$) symmetry.[5,6] To date, the electronic properties of the lanthanide oxyhydrides remain largely unexplored. A recent study by Ueda et al. suggests that Tb^{3+}-doped GdOH is a promising candidate for phosphor applications.[9]

A remarkable photochromic effect at ambient conditions was discovered in reactive magnetron sputtered (MS) YO_xH_y thin films.[10] Initially, these semiconducting materials (band gap $E_g \approx 2.6$ eV) were referred to as oxygen-containing yttrium hydride.[10,11] It was speculated that their properties can be explained in analogy to the transparent γ-YH_3 phase stabilized in the fcc structure by incorporation of oxygen into the lattice.[11] A later study on sputtered YO_xH_y composition gradient thin films, which covers the transition from opaque to transparent state, reports atomic ratios of up to $H/Y \approx 3$ as measured by heavy-ion elastic recoil detection (ERD) and nuclear reaction analysis (NRA).[12] However, this result seems rather questionable considering the low H_2 partial pressures during reactive MS deposition. Follow-up studies by Montero et al.[13] and Nafezarefi et al.[14] clarified that the transparent YO_xH_y materials are in fact formed by air oxidation of as-deposited absorbing metallic β-YH_2 films. Further, we reported that LnO_xH_y thin films with Ln = Gd, Dy, Er exhibit the same photochromic effect and fcc crystal structure as YO_xH_y.[14] On the basis of these findings and our preliminary chemical composition analysis experiments, we then adopted the term rare-earth (RE) *oxyhydrides* for this group of photochromic

Received: January 11, 2019
Accepted: February 20, 2019
Published: March 7, 2019

DOI: 10.1021/acs.jpclett.9b00088
J. Phys. Chem. Lett. 2019, 10, 1342−1348

materials. However, systematic experimental evidence for the presence of H^- ions in these REO_xH_y is scarce. Although a recent study by Moldarev et al. supports the concept of H^- in their photochromic YO_xH_y films, they also had to assume multiple cation charge states and/or the presence of OH^- complex ions in order to obtain charge balance.[15] Moreover, the relationship of the photochromic REO_xH_y thin films to the established group of stoichiometric LnOH bulk materials in terms of chemical composition and crystal structure remained unclear.

Here, we address these open questions by a combination of chemical composition analysis via ion beam methods, charge neutrality arguments, and optical characterization. We find that the photochromic REO_xH_y films are indeed *oxyhydrides*—clearly distinct from *hydroxides*—having a wide composition range along the MH_3–M_2O_3 axis. This allows us to explain their properties in the framework of O^{2-}/H^- anion-disorder, linking the known (anion-ordered) structures of REH_3 trihydrides, LnOH, and the RE_2O_3 sesquioxides.

Recently, we reported that metallic β-$MH_{1.9+\delta}$ dihydride thin films with M = Y, Er, Dy, Gd can be prepared by direct current (DC) reactive MS of metal targets in an Ar/H_2 atmosphere.[14] Above a certain material-dependent critical deposition pressure (p^*), the films air-oxidize at room temperature (RT) to form stable semiconducting transparent photochromic MO_xH_y. In order to obtain samples with a wide range of chemical compositions, we have extended our standard synthesis procedure as follows: (i) Sc is sputtered as the RE element with the smallest ionic radius. (ii) A variable amount of O_2 is added to the $Ar/H_2/O_2$ process gas (5N purity) resulting in a mixture containing (12.5–11.9) % of H_2 and (0–4.7) % of O_2. (iii) Pulsed DC plasma excitation (50 kHz, 90% duty cycle) is used to avoid arcing. (iv) Al capping layers (20 nm) were sputtered onto selected samples directly or after timed air exposure to prevent further oxidation. All samples were grown on unheated UV-grade fused silica (f-SiO_2) and polished glassy carbon substrates (HTW Germany). Structural and optical properties were investigated by a combination of X-ray diffraction (XRD, Bruker D8 Discover) and photospectrometry (PerkinElmer Lambda 900). A custom-built optical-fiber-based in situ spectrometer (range: 230–1150 nm) with attached 385 nm LED light source and a time resolution of ~1 s was employed to test the photochromic properties.

The MO_xH_y chemical composition is determined by a combination of Rutherford backscattering spectrometry (RBS) and ERD analysis at the 2 MV Van-de-Graaff accelerator at Helmholtz-Zentrum Dresden-Rossendorf (Dresden, Germany). RBS (ERD) measurements were performed with a 1.7 MeV $^4He^+$ beam at 0° (70°) incidence and 160° (30°) scattering angle using semiconductor detectors with a solid angle of 3.3 msr (5.6 msr) and an energy resolution of ~15 keV. The ERD detector was covered by a 6.6 μm Al stopper foil to discriminate recoiled H from forward scattered He. A special set of Sc, Y, and Gd dihydride reference samples was prepared by hydrogenating Pd-capped (20 nm) metal layers (150 nm) in a pressure cell at 1 bar of H_2 at RT. Employing the hydrogenography method,[16] the change in optical transmittance is used to verify that all films were initially loaded to H/M ratios above the dihydride to trihydride phase transition, followed by unloading to dihydride in air after opening the pressure cell. Because of the tensile strain induced by hydrogen desorption,[17] we expect that these dehydrogenated layers have a H/M ratio corresponding to the lower end of the β-MH_x existence range, i.e., $ScH_{1.68}$,[18] $YH_{1.90}$,[17] and $GdH_{1.80}$ (see Figures S1–S3 for XRD characterization). These dihydride samples turned out to be crucial to accurately calibrate the solid angle of the ERD detector. For each sample, the RBS and ERD spectra were fitted self-consistently using the SIMNRA[19] program and the SRIM2013 stopping power database.[20]

The result of this analysis is illustrated in Figure 1, showing the experimental ion beam spectra and corresponding

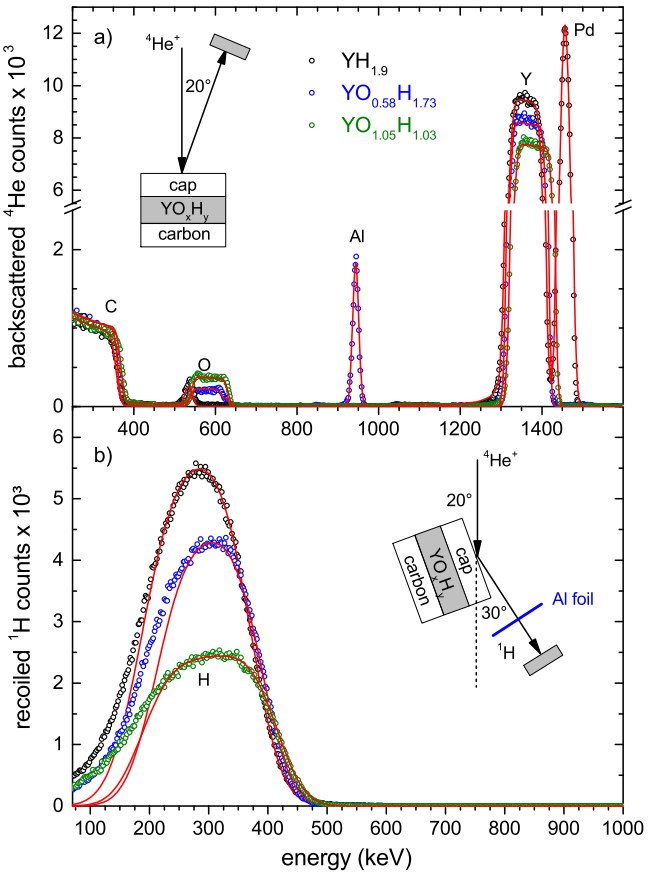

Figure 1. Comparison of (a) RBS and (b) ERD experimental spectra (open circles) and corresponding SIMNRA simulations (red lines) obtained by fitting of each combined data set. A series of samples (150 nm thickness) with increasing oxygen content is shown: Pd-capped Y dihydride (black), Al-capped (blue), and uncapped Y oxyhydride (green). The broadening of the low-energy edge in the ERD spectrum is caused by thickness variations of the Al stopper foil.

simulations of a set of YO_xH_y films with different O/H ratios. The areal densities (atoms/cm^2) of Y and O are obtained from RBS data, taking into account the Al or Pd capping layers. The overall fit accuracy benefits from the nearly background-free oxygen signal with good counting statistics, which is achieved by the use of carbon instead of f-SiO_2 substrates. The H areal density is obtained from the ERD signal taking into account the energy loss and straggling of H recoils in the Al stopper foil as well as geometric straggling[21] due to the variation of the scattering angle across the detector area. The combined RBS and ERD analysis allows for a quantification of the element concentrations (in atom %) with an uncertainty below 2 atom %. The RBS spectrum of Pd-capped hydrogenated Y shows that the film contains no oxygen (O detection limit 1 atom %) except for a thin surface layer within the C substrate

DOI: 10.1021/acs.jpclett.9b00088
J. Phys. Chem. Lett. 2019, 10, 1342–1348

- probably a result of surface polishing. It is important to note here, that no other light elements, in particular F, could be detected in the MO_xH_y films discussed in this work. Together with the previously observed characteristic transmittance window (Figure 5) and lattice constants,[14] this increases the confidence that our RE hydride samples are nearly ideal β-MH_x reference materials. Besides oxygen, fluorine is a common impurity in rare-earth metals - especially in Y.[22] In the past, we observed high concentrations of O (up to 7 atom %) and F (up to 13 atom %) in many commercial Y metal sputter targets of nominal 99.9% purity. Such high F concentrations complicate the chemical analysis and obscure subsequent interpretation of charge balance and electronic properties. Hence, we use high-purity Y targets supplied by Stanford Advanced Materials (United States) to avoid these problems.

The RBS and ERD simulations shown in Figure 1 confirm that the MO_xH_y film composition is homogeneous throughout the depth of the films. We have observed chemical gradients in a few samples prepared at deposition pressures far above the critical values of p^* = 0.3 Pa (Sc), 0.5 Pa (Y), and 0.7 Pa (Gd).[14] However, the interpretation of the composition−property relationships of such graded (and likely porous) films is rather ambiguous. Therefore, we have excluded these samples from further analysis.

Figure 2 shows the results of the ion beam chemical composition analysis of our $(Sc,Y,Gd)O_xH_y$ thin films in a generalized ternary M−O−H composition-phase diagram. This construction is based on the similar properties of the binary RE metal oxides and hydrides. At ambient conditions, the RE metals form stable M_2O_3 sesquioxides (except CeO_2) with a cubic bixbyite ($Ia\bar{3}$) structure (except La, Pr, and Nd).[23] All RE metals readily dissolve hydrogen, forming a random interstitial α-MH_x alloy where H occupies a fraction of the tetrahedral sites in the hexagonal close-packed (hcp) RE lattice. Upon hydrogenation, a phase transition to the metallic fcc ($Fm\bar{3}m$) β-MH_2 occurs for all REs. Further hydrogenation leads to a metal to insulator transition near H/M = 3. For most REs, this is accompanied by a structural phase transition to hcp γ-MH_3 (except Sc, La, Pr, Nd). Moreover, the REs form hcp $M(OH)_3$ hydroxides[25] and various MOOH oxy-hydroxide phases.

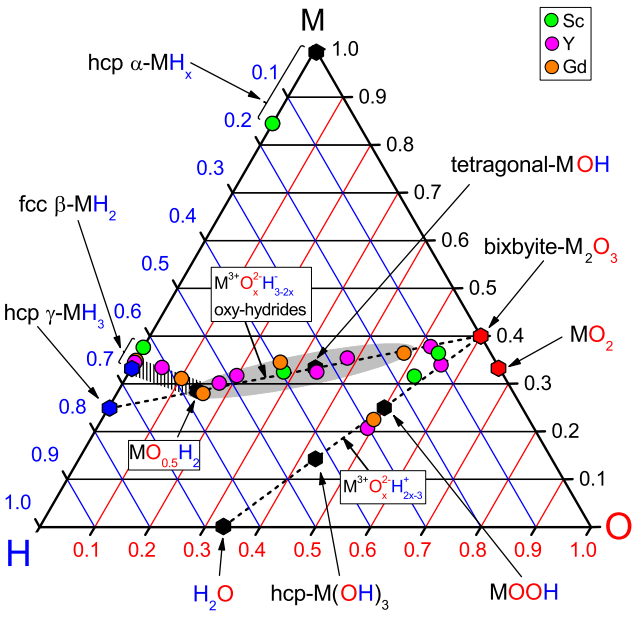

Figure 2. Ternary M−O−H chemical composition and phase diagram where M = Sc, Y ,La, Sm−Lu. Thick dashed lines indicate chemical compositions with the same charge state of cations (M^{2+}, M^{3+}, H^+) and anions (O^{2-}, H^-). Hexagons mark the (ideal) stoichiometric compounds that have been reported earlier: (i) binary compounds: MH_2 dihydride and MH_3 trihydride in blue as well as M_2O_3 sesquioxides[23,24] and MO_2 in red; (ii) ternary compounds: MOH oxyhydrides,[5−7] MOOH oxy-hydroxide, $M(OH)_3$ hydroxide,[25] and the hypothetical $MO_{0.5}H_2$ in black. Colored circles show the chemical compositions of MO_xH_y thin films obtained from ion beam analysis. Note that the diameter of the data points corresponds to a composition uncertainty of approximately ±1 atom %. The region of photochromic materials is highlighted in gray.

Our results show that the chemical composition of the Sc, Y, and Gd-based thin films follow the same general trends in the M−O−H diagram. Two material groups can be clearly distinguished by considering the formal valencies and demanding charge neutrality (indicated by dashed lines). The RE *oxyhydrides* with a composition range of $M^{3+}O_x^{2-}H^-_{3-2x}$ ($0.5 \leq x \leq 1.5$) are found on the line connecting MH_3 and M_2O_3. In particular, at x = 1 this includes the stoichiometric LnOH bulk compounds mentioned earlier. At x = 0.5, the data points deviate from the $M^{3+}O_x^{2-}H^-_{3-2x}$ line toward MH_2 (hatched area). This is consistent with our previous work showing that as-deposited films sputtered in Ar/H_2 are metallic dihydrides that oxidize in air to form transparent photochromic films.[14] We obtain gray opaque films with compositions between MH_2 and $MO_{0.5}H_2$ by sputtering at pressures near p^*. Their composition range in the ternary M−O−H diagram suggests that initially the air-oxidation proceeds via insertion of oxide ions into the MH_2 lattice accompanied by oxidation of M^{2+} cations to M^{3+}. The opaque character of these films is characteristic for intermixed metallic and dielectric phases indicating nucleation of semiconducting $MO_{0.5}H_2$ in β-MH_2. Note that $MO_{0.5}H_2$ (x = 0.5) marks the (ideal) composition where the conduction band is fully depleted of electrons (all cations are in the M^{3+} state) resulting in a metal−insulator transition that is observed in terms of the appearance of an optical band gap. Increasing the pressure above p^* or adding small amounts of O_2 during deposition leads to the formation of transparent semiconducting *oxyhydrides* with compositions between $MO_{0.5}H_2$ and M_2O_3. In contrast, the RE *hydroxides* with the composition range $M^{3+}O_x^{2-}H^+_{2x-3}$ ($1.5 \leq x \leq 3$) are located on the line connecting M_2O_3 and $M(OH)_3$. These transparent films were obtained by further increasing the O_2 fraction in the $Ar/H_2/O_2$ mixture during reactive sputtering.

XRD analysis confirms that all RE *oxyhydride* films in Figure 2 have fcc unit cell symmetry, where the lattice constant is expanded by (1.0−2.8)% relative to the dihydride because of oxygen incorporation (see XRD analysis in the Supporting Information). Moreover, the lattice constants of sputtered dihydrides, oxyhydrides, and oxides show a systematic variation with the RE ion radius according to the lanthanide contraction effect.[14] By combining the structural similarities of the known stoichiometric compounds and the chemical composition results, we propose a generalized simplified structure model for the RE *oxyhydrides* as shown in Figure 3. It is based on the fcc ($Fm\bar{3}m$) structure where the 4 lattice sites are occupied by the RE cations and the compounds differ only in the average anion occupation of the 8 tetrahedral and 4 octahedral interstices per unit cell. In this framework, the M_2O_3 oxides can be described by a random 6/8 occupation of

DOI: 10.1021/acs.jpclett.9b00088
J. Phys. Chem. Lett. 2019, 10, 1342−1348

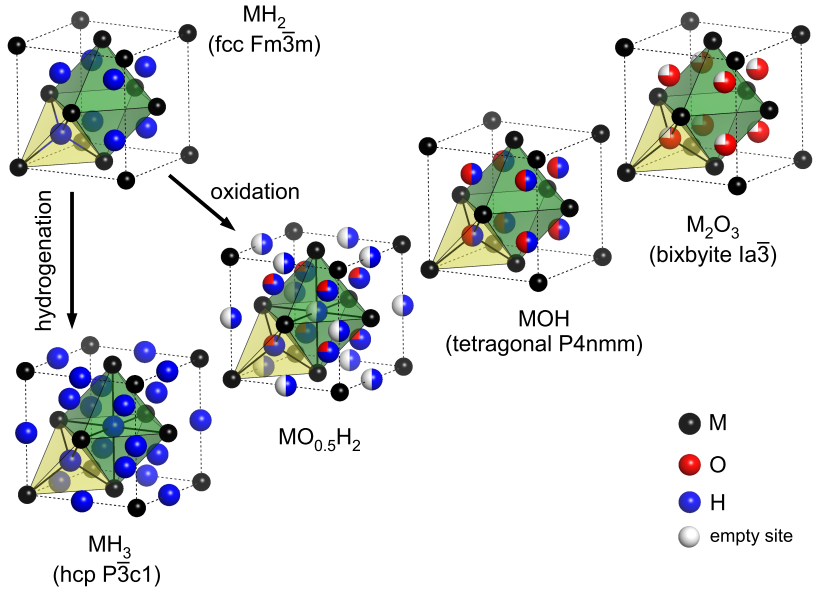

Figure 3. Generalized crystal structure evolution of rare-earth oxyhydrides with different H^-/M and O^{2-}/M ratios based on the fcc-fluorite ($Fm\bar{3}m$) structure motif. Anion sublattice disorder is visualized by multicolored spheres in terms of partial occupancy of tetrahedral (yellow polygon) and octahedral (green polygon) sites. The corresponding anion-ordered crystal structures of fcc-MH_2, hcp-MH_3, tetragonal MOH,[5,6] and bixbyite-M_2O_3[24] are given in parentheses. The arrows indicate metal−insulator transitions.

tetrahedral sites by O^{2-}, where anion-ordering would lead to a distortion of the fcc symmetry resulting in the bixbyite-M_2O_3 structure. The idealized structure of stoichiometric MH_2 is an fcc ($Fm\bar{3}m$) lattice where all 8 tetrahedral sites are occupied by H^- ions. Additional filling of the 4 octahedral sites by H^- leads to the idealized MH_3 structure. While the trihydrides of La, Ce, Pr, and Nd remain in the fcc structure up to H/M ≈ 3, the most common hcp structure of the RE γ-MH_3 can be interpreted as a distorted fcc lattice where the cubic (111) axis is parallel to the hcp *c*-axis. The structure of the stochiometric LnOH powder materials was previously described as a fcc ($Fm\bar{3}m$) where the tetrahedral sites are randomly occupied by O^{2-} and H^- with a 1:1 ratio.[7] The corresponding anion-ordered structure is tetragonal ($P4/nmm$).[5]

The resulting generalized picture of anion-disordered fcc symmetry as shown in Figure 3 illustrates that in the $M^{3+}O_x^{2-}H_{3-2x}^-$ *oxyhydrides* the cation-to-anion ratio changes from 1:1.5 in M_2O_3 to 1:3 in MH_3. This implies that the MOH composition (x = 1) marks a transition point regarding the occupation of tetrahedral and octahedral interstices. For x > 1, the octahedral sites are empty and additional structural tetrahedral vacancies are forming with increasing oxygen content up to a maximum amount of 25% in the M_2O_3 structure. In the case of x < 1, all tetrahedral sites are occupied and the octahedral sites are successively filled with hydride ions with increasing hydrogen content.

We observe photochromism of the *oxyhydrides* over a wide composition range for both x < 1 and x > 1, as shown by the highlighted gray area in Figure 2. However, the exact composition boundaries for photochromic MO_xH_{3-2x} remain unclear. Regarding the lower boundary, we did not obtain any oxyhydrides with x < 0.5 by either postoxidation of metallic β-MH_2 films or direct growth using oxygen-poor $Ar/H_2/O_2$ gas mixtures. This suggests that, in contrast to what was reported by You et al.,[12] H/M ratios above 2 in RE oxyhydride films cannot be achieved by reactive MS. This is because the typical H_2 partial pressures of a few 10 mPa during sputtering are far below the equilibrium pressure of the $MH_2 \rightarrow MH_3$ phase transition ($p_{H_2} \approx 0.1$ Pa)[26,27] and the addition of O_2 to the process gas favors further dehydrogenation. Therefore, we prepared a γ-$YH_{2.7+\delta}$ (x = 0) thin film by hydrogenation of a Pd-capped sputtered Y metal film at p_{H_2} = 3.2 kPa in a vacuum cell mounted into our in situ spectrometer. This trihydride did not show photochromism at RT, whereas air-oxidized RE dihydride films with $x \approx 0.5$ are photochromic. Hence, this value is marked as the O-poor boundary for photochromic RE *oxyhydrides* in Figure 2.

In order to discuss the O-rich boundary for photochromism, the effect of the anion ratio on optical properties has to be considered. Transmittance spectra of YO_xH_y films are presented in Figure 4. The dense YH_x film prepared at p = 0.3 Pa (i.e., far below the critical deposition pressure for Y) shows a transmittance window centered around 700 nm characteristic of metallic β-$YH_{1.9+\delta}$ dihydride, which is caused by a combination of weak interband and free-electron absorption.[28] The RE *oxyhydride* and hydroxide films are transparent semiconductors. The optical band gap of Y *oxyhydride* increases continuously with increasing O^{2-} content from (2.5 ± 0.1) eV at $x \approx 0.7$ up to (4.9 ± 0.2) eV at $x \approx 1.4$ (Figure 5). An extrapolation of this nonlinear trend (dashed line) leads to good agreement with the band gaps of Y_2O_3 (5.6 eV) and YH_3 (2.6 eV), which are determined by the O 2p → Y 3d and H 1s → Y 3d interband transition, respectively.[29] Therefore, the upper valence band of the RE *oxyhydrides* is likely formed by a mixture of occupied H 1s and O 2p states where the valence band maximum (VBM) shifts to lower energies with increasing O^{2-} concentration because of the higher electronegativity of oxygen (χ_O = 3.44) compared to hydrogen (χ_H = 2.20). The resulting band gap widening of the Y oxyhydrides does not depend linearly on the anion composition. This "band gap bowing" effect also occurs in many other semiconducting multianion compounds such as oxysulfides,[30,31] oxynitrides,[32] and III−V materials.[33] Its origin can be traced back to the mismatch in atomic orbital energy

DOI: 10.1021/acs.jpclett.9b00088
J. Phys. Chem. Lett. 2019, 10, 1342−1348

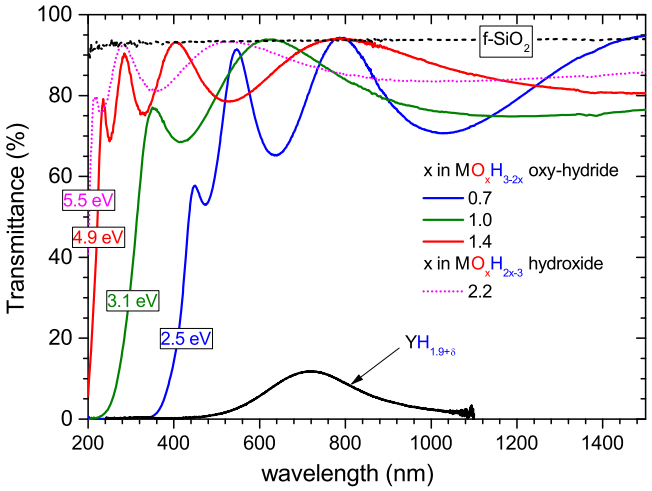

Figure 4. Transmittance spectra of Y-based ternary M−O−H films corresponding to Figure 2 with different compositions illustrating the metal−insulator transition from the dihydride $YH_{1.9+\delta}$ to the oxyhydride MO_xH_{3-2x} phase followed by band gap widening with increasing O^{2-}/H^- ratio. The transmittance of a hydroxide-like film with a large H^+ concentration of ∼30 atom % is shown for comparison. The optical band gap values as obtained from Tauc plots are given. The black dashed line is the transmittance of the bare fused silica substrate.

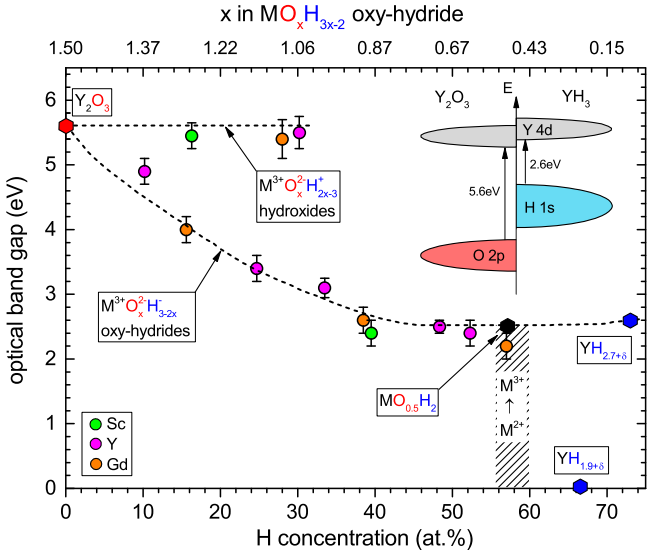

Figure 5. Dependence of the MO_xH_y optical band gap on the hydrogen concentration where M = Sc, Y, Gd (colored circles). Reported band gap values of the binary compounds Y_2O_3,[24] $YH_{2.7+\delta}$,[28] and metallic $YH_{1.9+\delta}$ are shown as colored hexagons. The metal−insulator transition upon oxidation of M^{2+} to M^{3+} with the hypothetical end point at $MO_{0.5}H_2$ is represented by the hatched region. Dashed lines are a guide to the eye and correspond to the charge-neutrality lines describing M^{3+} oxyhydrides and hydroxides in Figure 2. The fundamental electronic transitions of the binary end members of the Y oxyhydrides are illustrated.

and (an)ion size, which leads to coupling of electronic states affecting the relative positions of the VBM and the conduction band minimum (CBM) in random alloys.[34] It seems plausible that these established principles also apply to the electronic structure of the oxyhydrides. However, comprehensive studies on this topic are still lacking.

Figure 5 shows that the band gaps of the Sc- and Gd-based *oxyhydrides* follow the same trend as YO_xH_{3-2x}, which is reasonable considering the similarity in band gaps of the oxides: Sc_2O_3 (∼5.8 eV)[35] and Gd_2O_3 (5.4 eV)[36] as well as the trihydride GdH_3 (2.5 eV).[37] Slightly lower E_g values (−0.3 eV) for M = Sc, Gd are observed in *oxyhydrides* with low oxygen content ($x \approx 0.5$). This is in agreement with our work[14] on MO_xH_y with M = Y, Gd, Dy, Er and indicates that the effect of different RE cations on E_g is relatively weak compared to anion-alloying. Moreover, all RE *hydroxide* thin films have large optical band gaps ($E_g \approx 5.5$ eV) which are independent of the anion composition and similar in value to the sesquioxides, suggesting that the *unoccupied* H 1s orbitals do not interfere with the states at the VBM and CBM. Given the chemical similarity of the RE elements, we suppose that the anion-composition dependence of the optical band gap of most lanthanide *oxyhydrides* closely resembles the trend shown in Figure 5. Notable exceptions are expected for M = Ce, Pr, Eu, Tb where the M 4f orbitals are located within the O 2p → M 5d forbidden gap, resulting in a reduction of the M_2O_3 optical band gaps.[36,38]

Our ongoing photodarkening experiments with wavelength-dependent excitation indicate that photon energies larger than E_g are required to trigger photochromism in RE oxyhydrides. Using UV excitation by Hg vapor lamps with $\lambda = 254$ nm, we observe weak photochromism in YO_xH_{3-2x} *oxyhydrides* with band gaps up to 4.2 eV. According to Figure 5 this corresponds to $x = 1.3$ ($c_H \approx 15$ atom %) which is marked as the oxygen-rich boundary for photochromism in Figure 2.

In conclusion, we have established a ternary RE−O−H composition-phase diagram demonstrating that (i) the previously reported photochromic Y-based thin films[10,14] are O^{2-}/H^- multianion compounds which are members of the REO_xH_{3-2x} *oxyhydrides* material class including Sc and (most of) the lanthanides and that (ii) an anion-disordered fcc lattice model can be used to describe the crystal structure of the RE oxyhydrides linking the known REH_3, RE_2O_3, and LnOH[5−7] phases. These oxyhydride films are photochromic over nearly their entire composition range of $0.5 \leq x \leq 1.5$, which implies that the presence of *both* oxide and hydride ions is crucial for the photochromic effect at ambient conditions. We notice a general trend toward decreased photochromic contrast and faster bleaching kinetics with increasing O^{2-}/H^- ratio—in agreement with the report of Moldarev et al.[15] On the basis of our results, we expect that the stoichiometric bulk LnOH compounds ($x = 1$) should be photochromic as well. Moreover, the RE oxyhydride optical band gap can be adjusted over a wide range by controlling the O^{2-}/H^- anion ratio in order to adapt the photochromic response for applications such as energy-saving smart windows and adaptive eyewear. Further systematic investigation of the electronic structure and defect formation is required to clarify the origin and physical limitations of the photochromic effect in the REO_xH_y materials.

■ ASSOCIATED CONTENT

Supporting Information

The Supporting Information is available free of charge on the ACS Publications website at DOI: 10.1021/acs.jpclett.9b00088.

Structural characterization by XRD, SEM, and AFM and further experimental details (PDF)

DOI: 10.1021/acs.jpclett.9b00088
J. Phys. Chem. Lett. 2019, 10, 1342−1348

AUTHOR INFORMATION

Corresponding Author

*E-mail: s.cornelius@tudelft.nl. Phone: +31(0)1527-87391.

ORCID

Steffen Cornelius: 0000-0002-0358-7287
Giorgio Colombi: 0000-0001-6424-7684
Bernard Dam: 0000-0002-8584-7336

Notes

The authors declare no competing financial interest.

ACKNOWLEDGMENTS

The authors thank Dr. Nathan Nesbitt for facilitating access to the SEM and performing SEM measurements, Bart Boshuizen for programming the in-situ spectrometer control software, and Marcel Bus for performing AFM measurements. This work is part of the Open Technology research program with project number 13282, which is (partly) financed by The Netherlands Organisation for Scientific Research (NWO).

REFERENCES

(1) Kageyama, H.; Hayashi, K.; Maeda, K.; Attfield, J. P.; Hiroi, Z.; Rondinelli, J. M.; Poeppelmeier, K. R. Expanding frontiers in materials chemistry and physics with multiple anions. *Nat. Commun.* **2018**, *9*, 722.

(2) Hayward, M. A.; Cussen, E. J.; Claridge, J. B.; Bieringer, M.; Rosseinsky, M. J.; Kiely, C. J.; Blundell, S. J.; Marshall, I. M.; Pratt, F. L. The hydride anion in an extended transition metal oxide array: $LaSrCoO_3H_{0.7}$. *Science* **2002**, *295*, 1882−1884.

(3) Kobayashi, Y.; Hernandez, O.; Tassel, C.; Kageyama, H. New chemistry of transition metal oxyhydrides. *Sci. Technol. Adv. Mater.* **2017**, *18*, 905−918.

(4) Kobayashi, G.; Hinuma, Y.; Matsuoka, S.; Watanabe, A.; Iqbal, M.; Hirayama, M.; Yonemura, M.; Kamiyama, T.; Tanaka, I.; Kanno, R. Pure H^- conduction in oxyhydrides. *Science* **2016**, *351* (6729), 1314.

(5) Malaman, B.; Brice, J. F. Structural study of the hydride-oxide LaOH by X-ray diffraction and neutron-diffraction. *J. Solid State Chem.* **1984**, *53*, 44−54.

(6) Widerøe, M.; Fjellvag, H.; Norby, T.; Poulsen, F. W.; Berg, R. W. NdOH, a novel oxyhydride. *J. Solid State Chem.* **2011**, *184*, 1890−1894.

(7) Zapp, N.; Kohlmann, H. The lanthanide hydride oxides SmOH and HoOH. *Z. Naturforsch., B: J. Chem. Sci.* **2018**, *73*, 535.

(8) Yamashita, H.; Broux, T.; Kobayashi, Y.; Takeiri, F.; Ubukata, H.; Zhu, T.; Hayward, M. A.; Fujii, K.; Yashima, M.; Shitara, K.; et al. Chemical pressure-induced anion order-disorder transition in LnHO enabled by hydride size flexibility. *J. Am. Chem. Soc.* **2018**, *140*, 11170.

(9) Ueda, J.; Matsuishi, S.; Tokunaga, T.; Tanabe, S. Preparation, electronic structure of gadolinium oxyhydride and low-energy 5d excitation band for green luminescence of doped Tb^{3+} ions. *J. Mater. Chem. C* **2018**, *6*, 7541.

(10) Mongstad, T.; Platzer-Bjorkman, C.; Maehlen, J. P.; Mooij, L. P.; Pivak, Y.; Dam, B.; Marstein, E. S.; Hauback, B.; Karazhanov, S. Z. A new thin film photochromic material: oxygen-containing yttrium hydride. *Sol. Energy Mater. Sol. Cells* **2011**, *95*, 3596−3599.

(11) Mongstad, T.; Platzer-Bjorkman, C.; Karazhanov, S. Z.; Holt, A.; Maehlen, J. P.; Hauback, B. C. Transparent yttrium hydride thin films prepared by reactive sputtering. *J. Alloys Compd.* **2011**, *509*, S812−S816.

(12) You, C. C.; Moldarev, D.; Mongstad, T.; Primetzhofer, D.; Wolff, M.; Marstein, E. S.; Karazhanov, S. Z. Enhanced photochromic response in oxygen-containing yttrium hydride thin films transformed by an oxidation process. *Sol. Energy Mater. Sol. Cells* **2017**, *166*, 185−189.

(13) Montero, J.; Martinsen, F. A.; Lelis, M.; Karazhanov, S. Z.; Hauback, B. C.; Marstein, E. S. Preparation of yttrium hydride-based photochromic films by reactive magnetron sputtering. *Sol. Energy Mater. Sol. Cells* **2018**, *177*, 106−109.

(14) Nafezarefi, F.; Schreuders, H.; Dam, B.; Cornelius, S. Photochromism of rare-earth metal-oxy-hydrides. *Appl. Phys. Lett.* **2017**, *111*, 103903.

(15) Moldarev, D.; Moro, M. V.; You, C. C.; Baba, E. M.; Karazhanov, S. Z.; Wolff, M.; Primetzhofer, D. Yttrium oxyhydrides for photochromic applications: Correlating composition and optical response. *Phys. Rev. Mater.* **2018**, *2*, 115203.

(16) Gremaud, R.; Slaman, M.; Schreuders, H.; Dam, B.; Griessen, R. An optical method to determine the thermodynamics of hydrogen absorption and desorption in metals. *Appl. Phys. Lett.* **2007**, *91*, 231916.

(17) Remhof, A.; Kerssemakers, J. W. J.; van der Molen, S. J.; Kooij, E. S.; Griessen, R. Hysteresis in YH_x films observed with in-situ measurements. *Phys. Rev. B: Condens. Matter Mater. Phys.* **2002**, *65*, No. 054110.

(18) Manchester, F. D.; Pitre, J. M. The H-Sc system. *J. Phase Equilib.* **1997**, *18*, 194−205.

(19) Mayer, M. SIMNRA, a simulation program for the analysis of NRA, RBS and ERDA. *AIP Conf. Proc.* **1998**, *475*, 541−544 https://home.mpcdf.mpg.de/~mam/. .

(20) Ziegler, J.F.; Ziegler, M.D.; Biersack, J.P. SRIM 2013; 2013; www.srim.org.

(21) Szilagyi, E. Energy spread in ion beam analysis. *Nucl. Instrum. Methods Phys. Res., Sect. B* **2000**, *161−163*, 37−47.

(22) Takenouchi, A.; Otomo, K. N.; Sakai, M.; Saito, Y.; Kirigane, T.; Kosaka, M.; Michimura, S.; Hasegawa, S.; Nakamura, O. Purification of commercial yttrium metal: Removal of fluorine. *J. Cryst. Growth* **2017**, *468*, 701−704.

(23) Zinkevich, M. Thermodynamics of rare earth sesquioxides. *Prog. Mater. Sci.* **2007**, *52*, 597−647.

(24) Adachi, G.; Imanaka, N. The binary rare earth oxides. *Chem. Rev.* **1998**, *98*, 1479−1514.

(25) Beall, G. W.; Milligan, W.; Wolcott, H. A. Structural trends in the lanthanide trihydroxides. *J. Inorg. Nucl. Chem.* **1977**, *39*, 65−70.

(26) Kooij, E. S.; van Gogh, A. T. M.; Griessen, R. In situ resistivity measurements and optical transmission and reflection spectroscopy of electrochemically loaded switchable YH_x films. *J. Electrochem. Soc.* **1999**, *146* (8), 2990−2994.

(27) Huiberts, J. N.; Rector, J. H.; Wijngaarden, R. J.; Jetten, S.; de Groot, D.; Dam, B.; Koeman, N. J.; Griessen, R.; Hjörvarrson, B.; Olafsson, S.; et al. Synthesis of yttriumtrihydride films for ex-situ measurements. *J. Alloys Compd.* **1996**, *239*, 158−171.

(28) van Gogh, A. T. M.; Nagengast, D. G.; Kooij, E. S.; Koeman, N. J.; Rector, J. H.; Griessen, R.; Flipse, C. F. J.; Smeets, R. J. J. G. Structural, electrical, and optical properties of $La_{1-z}Y_zH_x$ switchable mirrors. *Phys. Rev. B: Condens. Matter Mater. Phys.* **2001**, *63*, 195105.

(29) Miyake, T.; Aryasetiawan, F.; Kino, H.; Terakura, K. GW quasiparticle band structure of YH_3. *Phys. Rev. B: Condens. Matter Mater. Phys.* **2000**, *61*, 16491−16496.

(30) Meyer, B. K.; Polity, A.; Farangis, B.; He, Y.; Hasselkamp, D.; Krämer, T.; Wang, C. Structural properties and bandgap bowing of $ZnO_{1-x}S_x$ thin films deposited by reactive sputtering. *Appl. Phys. Lett.* **2004**, *85*, 4929.

(31) Persson, C.; Platzer-Björkman, C.; Malmström, J.; Törndahl, T.; Edoff, M. Strong valence-band offset bowing of $ZnO_{1-x}S_x$ enhances p-type nitrogen doping of ZnO-like alloys. *Phys. Rev. Lett.* **2006**, *97*, 146403.

(32) Xie, R.; Hintzen, H. T. Optical properties of (oxy)nitride materials: A Review. *J. Am. Ceram. Soc.* **2013**, *96*, 665−687.

(33) Vurgaftman, I.; Meyer, J. R.; Ram-Mohan, L. R. Band parameters for III−V compound semiconductors and their alloys. *J. Appl. Phys.* **2001**, *89*, 5815.

(34) Wei, S.; Zunger, A. Band offsets and optical bowings of chalcopyrites and Zn-based II-VI alloys. *J. Appl. Phys.* **1995**, *78*, 3846.

(35) Afanas'ev, V. V.; Shamuilia, S.; Badylevich, M.; Stesmans, A.; Edge, L. F.; Tian, W.; Schlom, D. G.; Lopes, J. M. J.; Roeckerath, M.; Schubert, J. Electronic structure of silicon interfaces with amorphous

DOI: 10.1021/acs.jpclett.9b00088
J. Phys. Chem. Lett. 2019, 10, 1342−1348

and epitaxial insulating oxides: Sc_2O_3, Lu_2O_3, $LaLuO_3$. *Microelectron. Eng.* **2007**, *84*, 2278−2281.
(36) Prokofiev, A. V.; Shelykh, A. I.; Melekh, B. T. Periodicity in the band gap variation of Ln_2X_3 (X = O,S,Se) in the lanthanide series. *J. Alloys Compd.* **1996**, *242*, 41−44.
(37) Lee, M. W.; Lin, C. H. Determination of the optical constants of the y-phase GdH_3 thin films. *J. Appl. Phys.* **2000**, *87*, 7798.
(38) Gillen, R.; Clark, S. J.; Robertson, J. Nature of the electronic band gap in lanthanide oxides. *Phys. Rev. B: Condens. Matter Mater. Phys.* **2013**, *87*, 125116.

DOI: 10.1021/acs.jpclett.9b00088
J. Phys. Chem. Lett. 2019, 10, 1342−1348